Rate-Based Nonisothermal LLX Model and Its Experimental Validation

Debjit Sanpui, Manish K. Singh, and Ashok Khanna
Dept. of Chemical Engineering, Indian Institute of Technology Kanpur, Kanpur—208016 (U.P.), India

Most of the current open literature handles liquid–liquid extraction (LLX) using equilibrium and/or isothermal models. However, in most industrial applications, the assumption of equilibrium and isothermal operation is not reasonable. A rate-based nonequilibrium model for both the mass and energy transfer in LLX during the three distinct stages of drop formation—drop, fall or rise, and drop coalescence—has been developed. These three hydrodynamic phenomena affect the mass transfer between dispersed and continuous phases for which a parallel–parallel mass-transfer resistance model has been incorporated. Because of the very large number of computations associated with repeated calculations of mass-transfer coefficients a local model has been proposed. We have compared our rate-based simulator with two other commercial simulators and our bench-scale experiments have been done for toluene–acetone–water and methyl isobutyl ketone–acetic acid–water systems. Stagewise mass and energy transfer and the hydrodynamics features have been compared between the experimental and the simulation runs. Relative-error square analysis (for the concentration profiles) shows that our simulation results are two orders of magnitude better in comparison to other commercial simulators. © 2004 American Institute of Chemical Engineers *AIChE J,* 50: 368–381, 2004

Keywords: liquid-liquid extractions, rate-based model, mass-transfer resistances, local mass-transfer model, experimental validation

Introduction

The modeling of multicomponent liquid–liquid separation presented so far is based on the assumptions that equilibrium is achieved at each stage with respect to both heat and component mass-transfer. However, in most industrial applications, the assumption of equilibrium with respect to existing phase compositions and isothermal extraction operation is not reasonable. Several attempts have been made in this direction, such as those by Ricker and King (1981) and Spencer et al. (1981). In 1985, Krishnamurty and Taylor (1985) developed the first general *rate-based* computer-aided model for the application to tray and packed columns for distillation and other continuous, countercurrent vapor–liquid separation operations. Lao et al. (1989) also reported a *nonequilibrium*-stage model with respect to mass transfer for multicomponent liquid–liquid extraction. Krishnamurty and Taylor (1985) and Lao et al. (1989) had utilized drop diameter, number of drops, time of formation, rise and coalescence, and dynamic holdup in calculating mass-transfer coefficients, but these hydrodynamics features were neither tracked nor reported across each stage. They did not consider axial mixing across the stages. Apart from nonequilibrium, staged processes also experience the phenomenon of *back mixing* due to axial dispersion. Zimmerman et al.'s (1992) proposed model for extraction allows rigorous calculation of mass-transfer coefficients incorporating multicomponent interaction effect without considering the energy balance on the stages. Samant and Ng (1998) proposed the design of multistage extractive reaction processes for multicomponent systems.

An alternate rate-based approach is proposed to model the mass-transfer behavior of an extraction process. In the present

Correspondence concerning this article should be addressed to A. Khanna at akhanna@iitk.ac.in.

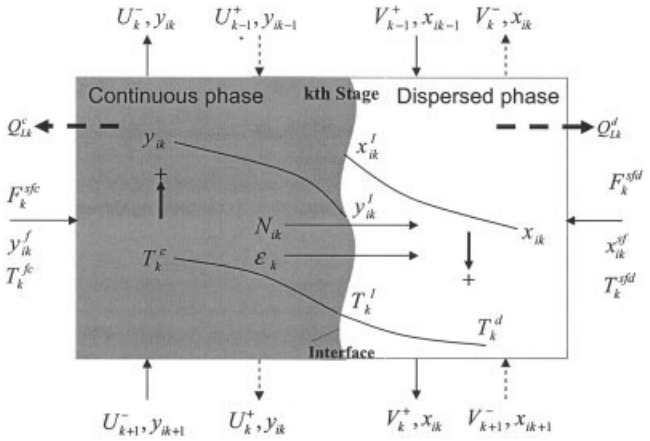

Figure 1. A nonequilibrium stage with heavy dispersed phase.

work our objective is to model the rate-based reactive non–isothermal liquid–liquid extraction process considering non-equilibrium with respect to both mass and energy transfer. Additionally *stage hydrodynamics* correlations and *back mixing* in both the phases have been taken into account. Mass-transfer resistance model for the three *drop phenomena*—drop formation, drop rise, and drop coalescence—also have been considered in the mass-transfer coefficient matrix.

Modeling of Extraction Process

The basic modeling equations for most of the separation processes are the MESH equations: mass conservation (M), equilibrium relationship (E), summation (S), energy balance (H). Two additional sets of equations—axial mixing ($\mathcal{A}$), and mass- and heat-transfer rate (**R**)—have been considered in the present liquid–liquid extraction model. The new set of model equations will now be MESH$\mathcal{A}$R equations.

Extraction involves two distinct phases: continuous and dispersed. The droplets formed in the process along with static holdup at the tray compose the dispersed phase. Back mixing is assumed in the form of axial dispersion between adjacent stages. The nonequilibrium stage is shown in Figure 1. In each stage the two liquid phases are brought into contact countercurrently from adjacent stages. In our model, we consider the drops of a single size and the drops move as a plug in contact with the bulk continuous phase. Each stage contains two phases, which are separated by an interface: a thin film of the corresponding phase exists on either side of the interface, and the interfacial mole fraction for the continuous (c-phase) and dispersed phase (d-phase) have been denoted as y^I_{ik} and x^I_{ik}, respectively. These films offer resistance for mass and heat transfer. The continuous phase also moves as a plug flow. The dynamic holdup of the dispersed phase at any stage k is represented by ϕ_k. The positive flow of the dispersed phase is denoted as V^+_k; since the continuous phase moves countercurrently in the opposite direction, positive flow is indicated by U^-_k. The back flows of the two phases are given by V^-_k and U^+_k; F^{sfd}_k and F^{sfc}_k represent the side feeds at stage k. The mass- and energy-transfer rates are denoted by N_{ik} and ε_k, and the direction of the mass and energy transfer is taken to be positive from the continuous to the dispersed phase; T^c_k, T^d_k, and T^I_k are the distinct temperatures of the continuous, dispersed, and interface, respectively, while Q^d_{LK} and Q^c_{LK} are the heat loss terms from the dispersed and continuous phase. A generalized reaction term, r_{kl}, has been considered in both phases to account for any chemical reaction during extraction. Briefly MESH$\mathcal{A}$R equations are as follows.

Mass Conservation Equations (M). Mass conservation equations with mass-transfer rate, back-mixing effects, side stream feed, and the phase reaction term

$$M^c_{ik}:\ U^+_{k-1}y_{ik-1} - (U^+_k + U^-_k)\,y_{ik} + U^-_{k+1}y_{ik+1} + F^{sfc}_k y^{sf}_{ik} - N_{ik} - \mathbf{V}^c_k \sum_{l=1}^{NRX} \nu_{il} r^c_{kl} = 0 \quad (1)$$

$$M^d_{ik}:\ V^+_{k-1}x_{ik-1} - (V^+_k + V^-_k)\,x_{ik} + V^-_{k+1}x_{ik+1} + F^{sfd}_k x^{sf}_{ik} + N_{ik} - \mathbf{V}^d_k \sum_{l=1}^{NRX} \nu_{il} r^d_{kl} = 0, \quad (2)$$

where the rate for the lth stage is

$$r_k = \sum_{p=1}^{2} k_p \prod_{q=1}^{NRC} (c_{kq}z_{kq})^m = \sum_{p=1}^{2} A_p \exp\left(\frac{-E_p}{RT^p_k}\right) \prod_{q=1}^{NRC} (c_{kq}z_{kq})^m \quad (3)$$

Phase Equilibrium Relationship (E). The bulk phases are not in equilibrium, but both the phases are in close contact such that equilibrium is assumed at the interface

$$E^I_{ik}:\ K_{ik}x^I_{ik} - y^I_{ik} = 0 \quad (4)$$

The distribution ratio, K, is estimated at the interface temperature T^I_k by either modified UNIFAC or UNIQUAC or NRTL models.

Summation Equations (S). Summation equations on the kth stage at the interfaces and bulk phases are given below

$$S^{Ic}_k:\ \sum_{i=1}^{NC} y^I_{ik} = 1.0; \qquad S^{Id}_k:\ \sum_{i=1}^{NC} x^I_{ik} = 1.0;$$

$$S^c_k:\ \sum_{i=1}^{NC} y_{ik} = 1.0; \qquad S^d_k:\ \sum_{i=1}^{NC} y_{ik} = 1.0 \quad (5)$$

Enthalpy Balance Equations (H). Enthalpy balance equations for both the phases have been written considering the heat of reaction and the heat loss from the stage

$$H^c_k:\ U^+_{k-1}H^c_{k-1} - (U^+_k + U^-_k)\,H^c_k + U^-_{k+1}H^c_{k+1} + F^c_k H^{fc}_k - \varepsilon^c_k - \mathbf{V}^c_k \sum_{l=1}^{NRX} \nu_{il} r^c_{kl} \Delta H^c_{rkl} - Q^c_{LK} = 0 \quad (6)$$

$$H_k^d:\ V_{k-1}^+ H_{k-1}^d - (V_k^+ + V_k^-) H_k^d + V_{k+1}^- H_{k+1}^d + F_k^d H_k^{fd} + \varepsilon_k^d - \mathbf{V}_k^d \sum_{l=1}^{NRX} \nu_{il} r_{kl}^d \Delta H_{rkl}^d - Q_{LK}^d = 0, \quad (7)$$

where

$$\varepsilon_k^d = \sum_{i=1}^{NC} N_{ik}^d H_{ik}^d + a_k h_k^d (T_k^I - T_k^d) \qquad \text{and}$$

$$\varepsilon_k^c = \sum_{i=1}^{NC} N_{ik}^c H_{ik}^c + a_k h_k^c (T_k^c - T_k^I) \quad (8)$$

The saturated liquid enthalpy for individual components and phases at temperature T_k^p has been calculated as follows

$$H_{ik}^p = H_{i,ref} + \int_{T_{ref}}^{T_k^p} C_{pik}\, dT \quad (9)$$

The enthalpy of the stream (continuous or dispersed phase) has been calculated as

$$H_k^p = \sum_{i=1}^{NC} z_{ik} H_{ik}^p + \Delta H_{mk}^p \quad (10)$$

where ΔH_{mk}^p, the heat of mixing in the individual phases, has been calculated from the Gibbs' free energy and entropy of mixture; these expressions are given in Appendix C (see Eq. C2).

Axial Mixing Relationships ($\mathcal{A}$).

$$\mathcal{A}_k^{c+}:\ U_k^+ - \left(\frac{D_k^c}{\Delta \hbar_k}\right)(1 - \phi_k) c_k^c A_o = 0 \quad (11)$$

$$\mathcal{A}_k^{c-}:\ U_k^- - \left(u_k^c + \frac{D_{k-1}^c}{\Delta \hbar_{k-1}}\right)(1 - \phi_k) c_k^c A_o = 0 \quad (12)$$

$$\mathcal{A}_k^{d+}:\ V_k^+ - \left(u_k^d + \frac{D_k^d}{\Delta \hbar_k}\right) \phi_k c_k^d A_o = 0 \quad (13)$$

$$\mathcal{A}_k^{d-}:\ V_k^- - \left(\frac{D_{k-1}^d}{\Delta \hbar_{k-1}}\right) \phi_k c_k^d A_o = 0 \quad (14)$$

There is no back-flow rate for the continuous phase in the topmost stage, and similarly no back flow for the dispersed phase in the bottommost stage.

Mass- and Heat-Transfer Rate Equations (R). As we have considered the rate-based process, the mass-transfer rate equation in both of the phases can be stated as follows:

$$R_{Mik}^c:\ (\mathrm{N})_k = y_{ik} \sum_{i=1}^{NC} N_{ik} + a_k [\boldsymbol{\kappa}]_k^c (y_{mk} - y_{mk}^I) \quad (15)$$

$$R_{Mik}^d:\ (\mathrm{N})_k = x_{ik} \sum_{i=1}^{NC} N_{ik} + a_k [\boldsymbol{\kappa}]_k^d (x_{mk}^I - x_{mk}). \quad (16)$$

Like the mass-transfer rates, the energy-transfer rates can be written as

$$R_{Ek}^I:\ \sum_{i=1}^{NC} (N_{ik}^c H_{ik}^c) + a_k h_k^c (T_k^c - T_k^I) - \left\{ \sum_{i=1}^{NC} (N_{ik}^d H_{ik}^d) + a_k h_k^d (T_k^I - T_k^d) \right\} = 0 \quad (17)$$

The $[\boldsymbol{\kappa}]_k^p$ matrices are functions of the binary mass-transfer coefficients, and the mole fractions of the components present in the multicomponent mixture and for nonideal system are shown in the Appendix.

Mass-Transfer Resistance Model

The rate of multicomponent mass transfer can be written in terms of Maxwell-Stefan mass transfer coefficients, k_{ij}, as suggested by Krishnamurty and Taylor (1985). In the extraction process, the mass transfer between continuous and dispersed phases occurs during drop formation, rise/fall, and coalescence. In our model, we have considered film on both sides of the interface; thus, the mass-transfer resistance is applicable in both the phases. The bulk concentration on each tray is assumed constant, that is, the concentrations of components in both phases do not change within the static and dynamic holdup. Sanpui and Khanna (2002) have suggested that the parallel–parallel mass-transfer resistance model matches well with the experimental results. A summary of the parallel mass-transfer-resistance model is given below.

Parallel-resistance model

It has been assumed that for the pth phase mass transfer stems from the interface (I) and bulk phase (b), and that all the three mass-transfer effects occur simultaneously, that is, in parallel. The parallel resistance model is shown in Figure 2. The total diffusive mass-transfer-rate equation based on the drop rise/fall area, a_{kr}, for all of the components on the kth stage for the pth phase can be written as follows

$$[\mathbf{J}]_{kt}^p = a_{kr} [\boldsymbol{\kappa}]_{kt}^p (z_k^{Ip} - z_k^{bp})_{av} \quad (18)$$

where $(z_k^{Ip} - z_k^{bp})_{av}$ is the vector (for the components $i = 1, \ldots, NC - 1$) of the difference of the interface and average bulk concentrations. Based on this assumption, all three phenomena (drop formation, rise/falling, and coalescence) have the same driving force on the kth stage; thus

$$\text{Drop formation } (f):\ [\mathbf{J}]_{kf}^p = a_{kf} [\boldsymbol{\kappa}]_{kf}^p (z_k^{Ip} - z_k^{bp})_{av} \quad (19)$$

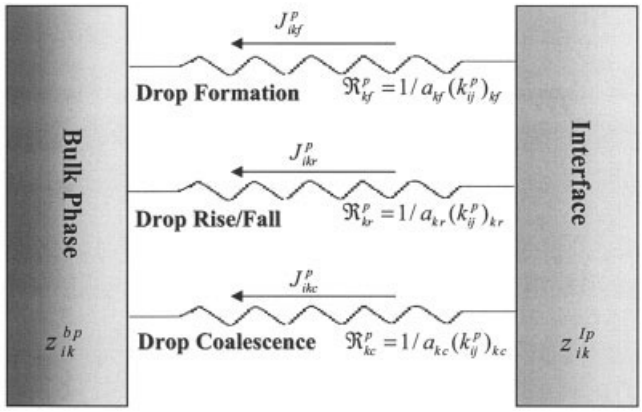

Figure 2. Parallel-resistance model.

$$\text{Drop rise or fall } (r): [\mathcal{J}]^p_{kr} = a_{kr}[\boldsymbol{\kappa}]^p_{kr}(z^{Ip}_k - z^{bp}_k)_{av} \quad (20)$$

$$\text{Drop coalescence } (c): [\mathcal{J}]^p_{kc} = a_{kc}[\boldsymbol{\kappa}]^p_{kc}(z^{Ip}_k - z^{bp}_k)_{av} \quad (21)$$

$[\boldsymbol{\kappa}]$ is presented in Eq. A30.

Based on the comparison, and taking individual transfer rates in Eqs. 19, 20, and 21 for the total diffusive mass transfer in Eq. 18, one can write the following resistance equation

$$\frac{1}{\Re^p_{kt}} = \frac{1}{\Re^p_{kf}} + \frac{1}{\Re^p_{kr}} + \frac{1}{\Re^p_{kc}} \quad (22)$$

Using the appropriate expression for the resistance terms, the net mass-transfer coefficient matrix can be calculated as

$$[\boldsymbol{\kappa}]^p_{kt} = c_{kf}[\boldsymbol{\kappa}]^p_{kf} + c_r[\boldsymbol{\kappa}]^p_{kr} + c_{kc}[\boldsymbol{\kappa}]^p_{kc}, \quad (23)$$

where

$$c_{fk} = \frac{a_{kf}}{a_{kr}}, \qquad c_r = 1.0, \qquad c_{ck} = \frac{a_{kc}}{a_{kr}} \quad (24)$$

It has been observed that 90% of the mass transfer takes place during drop rise. In Eqs. 23 and 24 the reference mass-transfer area is taken as the mass-transfer area for drop rise, that is, a_{kr}.

Mass-Transfer Areas. Areas for the three different drop phenomena are given as:

Drop formation area:

$$a_{fk} = n_0 \pi d^2_{pk} \quad (25)$$

Drop fall/rise area:

$$a_{rk} = \frac{6(A_0 - A_D)(\hbar_{sg} - \hbar_{ck})\phi_k}{d_{pk}} \quad (26)$$

Drop coalescence area:

$$a_{ck} = A_0 - A_D \quad (27)$$

The expression for the *constitutive equations*—mass transfer, heat transfer, and the associated hydrodynamic parameters—used in the present rate-based nonisothermal model are given in the Appendix. The earlier models for liquid–liquid and

Table 1. LLX and VLE Models and Their Features

Model Equations (per Stage)	Symbol	Kehat and Ghitis (1981)	Taylor and Krishna (1985) [VLE]	Powers et al. (1988) [VLE]	Lao et al. (1989)	Zimmermann et al. (1995)	Our Model*
1. Overall mass balance	M^1_{Ok}, M^2_{Ok}	√	√		√		
2. Component mass balance	M^1_{ik}, M^2_{ik}	√	√	√	√	√	√
3. Equilibrium relationship	E^I_{ik}	√	√	√	√	√	√
4. Summation equations (bulk)	S^1_k, S^2_k	√		√		√	√
5. Summation equations (interface)	S^{I1}_k, S^{I2}_k		√			√	√
6. Energy balance	H^1_k, H^2_k		√	√			√
7. Interface mass-transfer rate	R^{I1}_{Mk}, R^{I2}_{Mk}		√	√	√	√	√
8. Interface energy transfer rate	R^I_{Ek}		√	√			√
9. Axial mixing equations	A^{1+}_k, A^{1-}_k, A^{2+}_k, A^{2-}_k					√	√
10. Hydraulic equation	P_k		√				√
11. Hydrodynamic relations	$\mathcal{H}_k$					√	√
Model Variables (per Stage)	**Symbol**						
1. Forward mole flow rates (total)	V^+_k, U^-_k	√	√		√	√	√
2. Forward component mole flow	v^+_{ik}, u^-_{ik}			√			
3. Backward mole flow rates	V^-_k, U^+_k					√	√
4. Mole fractions (bulk)	x_{ik}, y_{ik}	√	√		√	√	√
5. Temperatures (bulk)	T^1_k, T^2_k		√	√			√
6. Mass transfer rate	N_{ik}		√	√	√	√	√
7. Mole fraction (interface)	x^I_{ik}, y^I_{ik}		√	√	√	√	√
8. Temperatures (interface)	T^I_k		√	√			√
9. Phase velocity	u^2_k					√	√
10. Holdup	ϕ_k					√	√
11. Pressure	P_k		√				√

* *Constitutive equations:* Heat of mixing; local mass-transfer model; heat loss; convergence criterion.
Notation: 1: vapor/light phase; 2: liquid/heavy phase; y: vapor/light phase composition; x: liquid/heavy phase composition.

Table 2. Equation and Variable Vector Order

Reference	Equation Vector	Number of Equations
Kehat and Ghitis (1981)	Not reported	$2NC + 2$
Taylor and Krishna (1985) [VLE]	M^1_{Ok}, M^1_{ik}, H^1_k, R^{I1}_{Mk}, S^{I1}_k, E^I_{ik}, R^I_{Ek}, M^2_{Ok}, M^2_{ik}, H^2_k, R^{I2}_{Mk}, S^{I2}_k, P_k	$6NC + 8$
Powers et al. (1988) [VLE]	M^1_{ik}, H^1_k, H^2_k, M^2_{ik}, R^{I1}_{Mk}, R^I_{Ek}, E^I_{ik}, R^{I2}_{Mk}	
Lao et al. (1989)	M^1_{Ok}, M^1_{ik}, M^2_{Ok}, M^2_{ik}, R^{I1}_{Mk}, E^I_{ik}, R^{I2}_{Mk}	$5NC$
Zimmermann et al. (1995)	Not reported	$4NC\ ND + 3ND + NC + 3$
Our model	S^{I2}_k, S^{I1}_k, S^2_k, S^1_k, E^I_{ik}, R^{I2}_{Mk}, R^{I1}_{Mk}, H^2_k, H^1_k, $\mathcal{A}^{2+}_k$, $\mathcal{A}^{2-}_k$, $\mathcal{A}^{1+}_k$, $\mathcal{A}^{1-}_k$, M^2_{ik}, M^1_{ik}, R^I_{Ek}	$5NC + 9$

Reference	Variable Vector	Number of Variables
Kehat and Ghitis (1981)	Not reported	$2NC + 2$
Taylor and Krishna (1985) [VLE]	U^-_k, y_{ik}, T^1_k, y^I_{ik}, x^I_{ik}, T^I_k, V^+_k, x_{ik}, T^2_k, N_{ik}, P_k	$6NC + 8$
Powers et al. (1988) [VLE]	u^-_{ik}, T^1_k, T^2_k, v^+_{ik}, N_{ik}, y^I_{ik}, T^I_k, x^I_{ik}	
Lao et al. (1989)	U^-_k, y_{ik}, V^+_k, x_{ik}, N_{ik}, y^I_{ik}, x^I_{ik}	$5NC$
Zimmermann et al. (1995)	Not reported	$4NC\ ND + 3ND + NC + 3$
Our model	x^I_{ik}, y^I_{ik}, T^I_k, N_{ik}, V^+_k, U^-_k, V^-_k, U^+_k, T^2_k, T^1_k, ϕ_k, u^2_k, x_{ik}, y_{ik}	$5NC + 9$

Notation: 1: vapor/light phase; 2: liquid/heavy phase; y: vapor/light phase composition; x: liquid/heavy phase composition.

vapor–liquid systems, along with the present model, are compared in Table 1.

Steady-State Simulation

The simulation model described is a set of nonlinear equations, which has to be solved by using the multivariable Newton-Raphson (N-R) method. Three enthalpy balance equations have been scaled by a factor of 10^5 (order of magnitude of enthalpy). A computer code has been written in C language for this purpose, to solve steady-state simulation of the multicomponent sieve tray column. The N-R method for solving the set of nonlinear equations is found to be very stable. Let ($\mathbf{F}(\mathbf{X})$) denote the vector (as in Table 2) of nonlinear equations (Eqs. 1 to 17) to be solved for the vector of independent variables $\mathbf{X} \equiv (\mathbf{X}_1, \mathbf{X}_2, \ldots, \mathbf{X}_n)$, with solution ($\mathbf{F}(\mathbf{X})$) $\equiv$ ($\mathbf{0}$). Then the N-R method suggests the solution $\mathbf{X}^{n+1}$ by the following relation (Eq. 29). This method requires the calculation of the Jacobian, which involves partial derivatives of equations with respect to independent variables. These independent variables are listed in Eqs. 32 and 34, and are denoted here by the single vector $\mathbf{X}$. A vector $\mathbf{D}$ that contains the residuals of the corresponding equations represents the righthand sides of all the modeling equations. The well-known sparse equation solver *Thomas algorithm* has simultaneously solved the linearized system of equations (with a block-tridiagonal coefficient matrix) quite efficiently. The block Thomas algorithm solves the linearized system of equations to yield the vector ($\Delta\mathbf{X}^n$). Thence, the solution vector for the nth iteration is obtained as

$$\Delta\mathbf{X}^n = -\mathbf{J}^{-1}\mathbf{D}. \tag{28}$$

The simulation variables $\mathbf{X}$ are updated as

$$\mathbf{X}^{n+1} = \mathbf{X}^n + \lambda(\Delta\mathbf{X}^n), \tag{29}$$

where λ is evaluated by optimization such as by the Golden Section method, in which case its value lies between 0 and 1. The following criterion has been used to check the convergence of the iterative method

$$\sum_{k=1}^{NS}\left(\sum_{q=1}^{NE}\mathbf{F}^2_{qk}\right) < \tau, \tag{30}$$

that is, the sum of the squares of the function residuals should be less than some tolerance τ. For steady-state simulation, tolerance τ is taken as 10^{-6}, which takes care of both mass- and energy-balance errors of the simulation. It has been observed that in the LLX simulation for a large number of components and a large number of stages *convergence of only enthalpy balance equations* [for the continuous, dispersed phase, and interface equations (Eqs. 6, 7, and 17)] per stage is sufficient for convergence of all the other model equations. Thus, Eq. 30 can be rewritten as

$$\sum_{k=1}^{NS}\left(\sum_{q=1}^{3}\mathbf{F}^2_{qk}\right) < \tau, \tag{31}$$

Table 3. Comparative Computational Times

Sl. Number	Operations	Run Time* with Local Model	Run Time* with Rigorous Model	Time Gain Factor
1	*Lab-scale column:* eight stages; three components	5 s	60 s (1 min)	12
2	*Pilot-scale column:* forty stages; three components	40 s	400 s (6.67 min)	10
3	*Pilot-scale column:* forty stages; six components	60 s (1 min)	900 s (15 min)	15
4	*Plant-scale column:* fifty-seven stages; three components	120 s (2 min)	2400 s (40 min)	20
5	*Plant-scale column:* fifty-seven stages; six components	200 s (3.33 min)	5000 s (83.33 min)	25

* Run time for total column convergence without printing.

Table 4. Column and Feed Specification

Column specification	
Column diameter	0.102 m
Number of stages	8
Sieve tray spacing	0.2 m
Number of holes (sieve)	120
Sieve hole diameter	0.00318 m
Feed location	
Feed*	@ 8 stage (bottom)
Solvent**	@ 1 stage (top)

* Toluene–acetone for TAW system; MIBK + acetic acid for MAW system.
** Solvent is water for both TAW and MAW systems.

where q denotes the three energy-balance equations: continuous, dispersed, and interface. Convergence on only energy balance equations (Eqs. 6, 7, and 17) brings down the simulation time to 20–30% of the original.

Block reordering procedure

In solving the model equations for the nonequilibrium-stage model of multicomponent separations, Taylor and Krishna (1985), Powers et al. (1988), and Lao et al. (1989) have not outlined the procedures involved in the ordering of the simulation variables and the model equations. However, all the previous workers have utilized their own particular order for solving the model equations as given in Table 2. In our model, the initial order as used by Jaiswal (1999) is given by Eqs. 32 and 33:
Variable vector:

$$(\mathbf{X}_k)^T \equiv (V_k^+, V_k^-, U_k^+, U_k^-; x_{ik}, y_{ik}; T_k^d, T_k^c; x_{ik}^I, y_{ik}^I; N_{ik}; \phi_k, u_k^c; T_k^I). \quad (32)$$

Equation vector:

$$(\mathbf{F}_k)^T \equiv (M_{ik}^d, M_{ik}^c; \mathcal{A}_k^{d+}, \mathcal{A}_k^{d-}, \mathcal{A}_k^{c+}, \mathcal{A}_k^{c-}; H_k^d, H_k^c; R_{Mk}^{Id}, R_{Mk}^{Ic}; E_{ik}^I; S_k^d, S_k^c, S_k^{Id}, S_k^{Ic}; R_{Ek}^I). \quad (33)$$

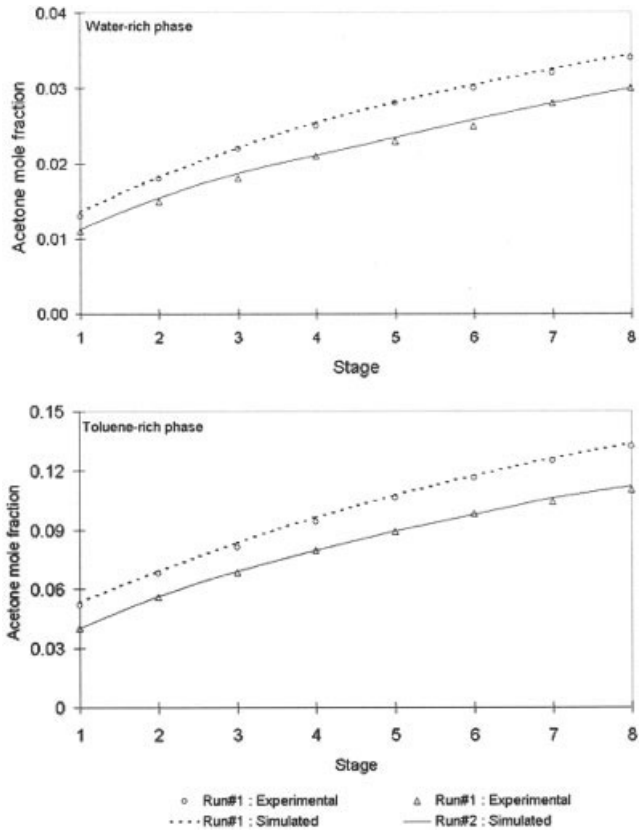

Figure 3. Acetone profiles in continuous and dispersed phases for TAW system.

The variable vector along the column and the equation vector along the row arrange themselves in a 7×7 matrix per stage.

Matrix inversion of the highly sparse Jacobian matrix $\mathbf{J}$ led to singularity. Hence a reordering procedure of the sparse matrix had to be adopted, as suggested by Markowitz (1957) and Stadtherr and Wood (1984a,b). In the Markowitz method of sparse-matrix reordering, forward (or backward) triangularization has been done with a minimum column (or row count),

Table 5. Bench-Scale LLX Run Details

Run Number	Systems	Phases (Feed to the LLX Column)		S/F	$\Delta T = T_{in}^d - T_{in}^c$
		Continuous	Dispersed		
1	TAW*	Acetone = 15% Toluene = 85% T_{in}^d = 33°C	Water = 100% T_{in}^c = 50°C	3	17
2	TAW	Acetone = 15% Toluene = 85% T_{in}^d = 33°C	Water = 100% T_{in}^c = 50°C	4	17
3	MAW**	Acetic acid = 7.15% MIBK = 90.85% Water = 2.0% T_{in}^d = 33.5°C	Water = 100% T_{in}^c = 50°C	2	16.5
4	MAW	Acetic acid = 7.15% MIBK = 90.85% Water = 2.0% T_{in}^d = 33.5°C	Water = 100% T_{in}^c = 50°C	3	16.5

* TAW—toluene–acetone–water.
** MAW—Methyl isobutyl ketone (MIBK)–acetic acid–water.

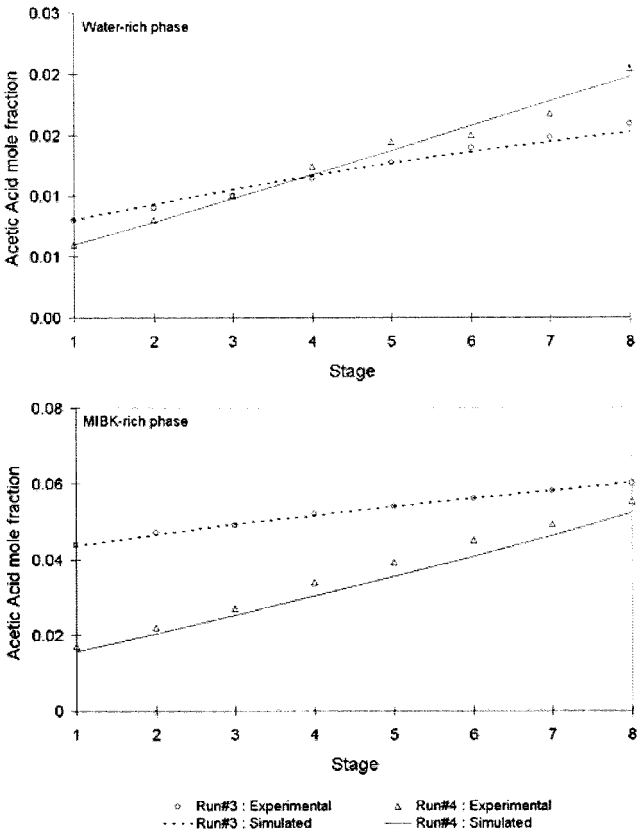

Figure 4. Acetic acid profiles in continuous and dispersed phases for MAW system.

respectively. The final order obtained using this procedure is presented below:
Variable vector:

$$(\mathbf{X}_k)^T \equiv (x_{ik}^I, y_{ik}^I; T_k^I; N_{ik}; V_k^+, V_k^-, U_k^+, U_k^-; T_k^d, T_k^c; \phi_k, u_k^c; x_{ik}, y_{ik}) \tag{34}$$

Equation vector:

$$(\mathbf{F}_k)^T \equiv (S_k^{Id}, S_k^{Ic}, S_k^d, S_k^c; E_{ik}^I; R_{Mk}^{Id}, R_{Mk}^{Ic}; H_k^d, H_k^c; \mathcal{A}_k^{d+}, \mathcal{A}_k^{d-}, \mathcal{A}_k^{c+}, \mathcal{A}_k^{c-}; M_{ik}^d, M_{ik}^c; R_{Ek}^I) \tag{35}$$

Local mass-transfer model

The expressions for the binary diffusivities and mass-transfer coefficients are complicated functions of basic physical properties and are time-consuming to use in the rigorous simulator. Powers et al. (1988) have mentioned that the calculation of derivatives of the mass-transfer rate equations is the most time-consuming part of the simulation, demanding about 35% of the total computational time. They have also found that the binary mass-transfer coefficients do not change very much from tray to tray or from iteration to iteration, even though the composition and temperature change considerably. They have suggested that the calculation of derivatives of the mass-transfer coefficient can be neglected in inner iterations. Unfortunately, they have not mentioned the expressions for the binary

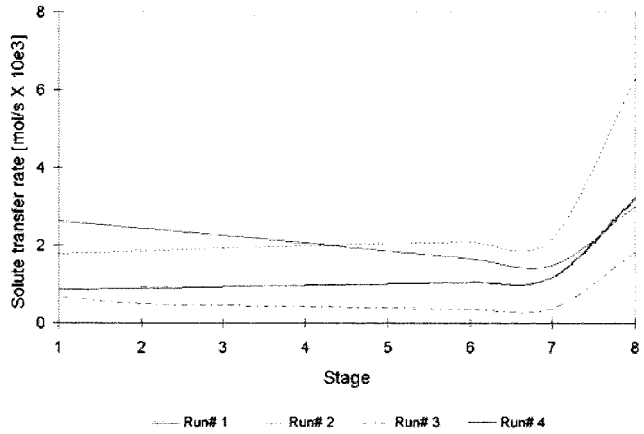

Figure 5. Solute transfer-rate profiles for TAW and MAW systems.

mass-transfer coefficients and they have not considered the three mass-transfer coefficients for the three different drop phenomena. For a simulation with a large number of components in an industrial liquid–liquid extraction column (more than 50 stages), there are more than a million "calls" on the diffusivity and mass-transfer coefficient functions in a single iteration. Completion of a full rigorous simulation of an industrial column takes more than two hours using a Pentium III, 1-GHz workstation. To make the calculation faster, a novel technique of a local mass-transfer model has been proposed here. The local model approach has been used for the calculation of nonideal multicomponent LLE phase equilibria, as suggested by Chimowitz et al. (1984) and for thermodynamic property by Hillestad et al. (1989). In this work, a simple expression has been proposed for the local model of the mass-transfer coefficient. This expression has been used in the inner iterations of simulation when the basic physical properties (such as the phase density, phase viscosity, phase molecular weight, and the interfacial tension) do not change more than 0.1% of the previous iteration value. If the change in any of the basic properties is more than 0.1%, then the simulator uses the actual detailed mass-transfer coefficient expression. The expression used for the local mass-transfer coefficient as a function of the Sherwood number is given as

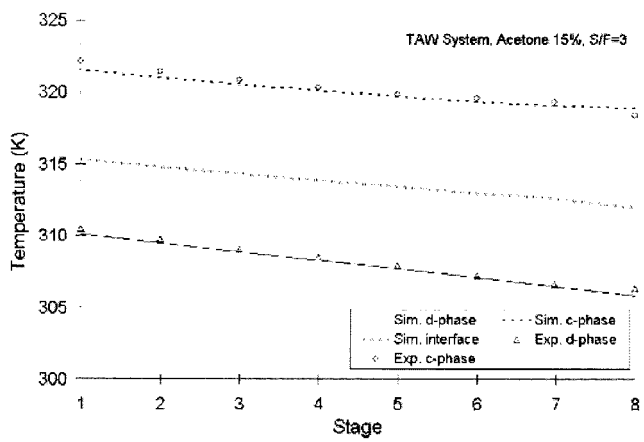

Figure 6. Temperature profiles for TAW system.

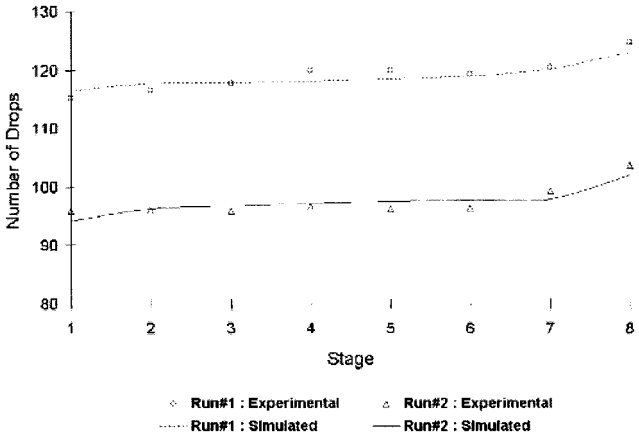

Figure 7. Profiles of number of drop for TAW system.

$$[(k_{ij}^{p})_{k}^{local}]^{n+1} = [(Sh_{ij}^{p})_{k}]^{n}\left[\left(\frac{c^{p}\mathcal{D}_{ij}^{p}}{d_{p}}\right)_{k}\right]^{n+1} \qquad (36)$$

After introducing the local model for the mass-transfer coefficient calculation, the simulation runs are much faster than before.

A brief comparison study for the time-gain factor using the local mass-transfer model has been presented for different column simulations in Table 3. It is seen that 10 to 25 times of simulation time is saved after incorporation of the local model (Eq. 36).

Validation of the Model

The rate-based model just discussed has been computer coded and the simulation package LLXSIM has been developed. The model can be used to study the bench-scale, pilot-scale, and industrial-size liquid–liquid extraction columns for analysis of product streams, troubleshooting and de-bottlenecking operations. Although we have incorporated the phase-reaction terms in the mass- and enthalpy-balance equations, we have not considered any reactive extraction process in the present work. For the validation of the model a bench-scale LLX column was commissioned and experiments with two different systems [toluene–acetone–water (TAW) and methyl isobutyl ketone (MIBK)-acetic acid–water (MAW)] were performed. The components for the TAW system could be separated by simple distillation, but the MAW system components could not be separated by simple distillation because of azeotrope formation. The developed rate-based simulation package LLXSIM has been run for the same experimental conditions, and simulated and experimental profiles have been compared.

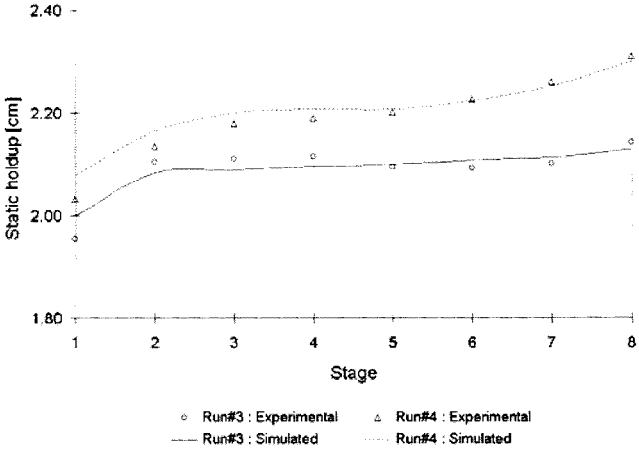

Figure 8. Static holdups with stages for MAW system.

Bench-scale experiments

The liquid–liquid extraction was studied in a 10.2-cm-diam sieve tray column; total length of the column is 1.78 m with 8 stages. A cylindrical down-comer (length 13 cm and diameter 17 mm) made of glass was fixed in each tray. To avoid corrosion stainless steel and Teflon pipelines were used. To draw the samples for both phases, separate sample ports have been provided at each stage in the glass column. In these studies, the heavy phase is fed from the top and the light dispersed phase from bottom of the column. A spiral-shaped distributor was used to disperse the light phase at the bottom of the column. Brief column and feed specifications are shown in Table 4. At the start of the run, the column was filled with heavy continuous phase approximately up to the continuous phase inlet. Then the light dispersed phase line was opened. When the light phase has reached the topmost stage, the heavy phase line was also opened. The steady-state condition is indicated by the constant height of the coalesced layer in each tray. After attaining the steady state of the column, samples

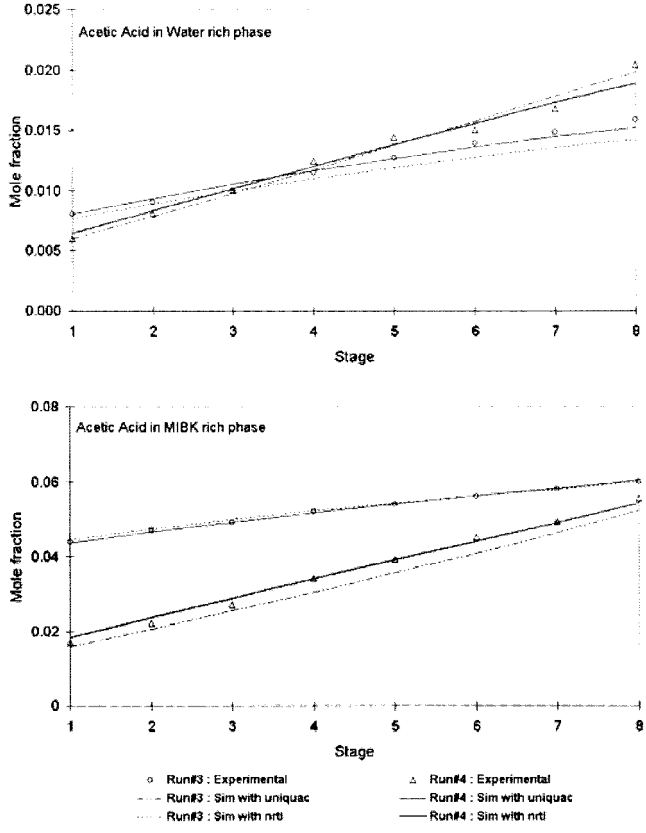

Figure 9. Acetic acid profiles with different thermodynamic models for MAW system.

Table 6. Relative Error-Squares with Different Simulation Options

Mol % Acetone in Feed	S/F	LLXSIM_Q	LLXSIM_N	CS_NE_Q**	CS_NE_N	CS_E_Q	CS_E_N†	Aspen_Q[1]	Aspen_N[2]
[Acetone in the Water Phase]									
Feed temp. = 32°C; Solvent temp. = 40°C									
10	3	0.0026	0.0022	0.1158	0.1385	0.0316	0.4153	0.0316	0.4151
10	4	0.0026	0.0028	0.1688	0.1902	0.0956	0.6406	0.0956	0.6405
15	3	0.0012	0.0006	0.1169	0.1242	NC*	0.2232	0.0321	0.2230
15	4	0.0019	0.0013	0.1772	0.1870	0.1024	0.6177	0.1025	0.6177
Feed temp. = 33°C; Solvent temp. = 50°C									
10	3	0.0017	0.0020	0.1234	0.1426	0.0266	0.3840	0.0266	0.3834
10	4	0.0019	0.0016	0.1895	0.2051	0.1013	0.6247	0.1013	0.6246
15	3	0.0009	0.0004	0.1351	0.1388	NC	0.1792	0.0192	0.1789
15	4	0.0010	0.0005	0.2015	0.2076	NC	0.6004	0.1159	0.6004
Mean RESQ		0.0017	0.0014	0.1535	0.1667	0.0715	0.46063	0.0656	0.4604
[Acetone in the Toluene Phase]									
Feed temp. = 32°C; Solvent temp. = 40°C									
10	3	0.0003	0.0002	0.0146	0.0091	0.0319	0.5689	0.0319	0.5688
10	4	0.0029	0.0024	0.0820	0.0135	0.1008	0.7523	0.1008	0.7522
15	3	0.0004	0.0000	0.0115	0.0025	NC	0.3035	0.0344	0.3031
15	4	0.0004	0.0008	0.0362	0.0122	0.1250	0.7257	0.1250	0.7257
Feed temp. = 33°C; Solvent temp. = 50°C									
10	3	0.0002	0.0000	0.0168	0.0056	0.0315	0.5319	0.0315	0.5312
10	4	0.0118	0.0103	0.1387	0.0356	0.0867	0.7293	0.0867	0.7291
15	3	0.0009	0.0003	0.0167	0.0009	NC	0.2482	0.0386	0.2477
15	4	0.0001	0.0001	0.0549	0.0185	NC	0.7028	0.1162	0.7027
Mean RESQ		0.0021	0.0017	0.0464	0.0122	0.0751	0.5703	0.0706	0.5700

[1] ASPENPLUS run in nonequilibrium mode with UNIQUAC interaction parameters.
[2] ASPENPLUS run in nonequilibrium mode with NRTL interaction parameters.
* NC–Not converged.
** CHEMSEP run in nonequilibrium mode with UNIQUAC interaction parameters.
† CHEMSEP run in equilibrium mode with NRTL interaction parameters.

from all eight stages were collected and kept in airtight glass bottles. The column was operated for 45 min for each run. All the samples were analyzed on a gas chromatograph (GC) with the Porapac-Q packed column (SS column, 1/8″ OD, 1.5 m length). The GC was operated in isothermal mode at 200°C oven temperature and 210°C detector (TCD) temperature. In the present work, four different LLX runs have been considered and details of the runs are shown in Table 5. Considering the basic features of the rate-based model for the liquid–liquid extraction, the model validation with the bench-scale experimentation work was carried out through four major aspects, as given below.

Mass-Transfer Features. Samples for both ternary systems (TAW and MAW) were taken from each stage and analyzed on GC. Comparative mole-fraction profiles of acetone in the water and toluene phases (for the TAW system), and the acetic acid in water and MIBK phases (for the MAW system) for both the experiment and simulation are shown in the Figures 3 and 4, respectively. It can be observed that the experimental data points of the TAW and MAW systems closely match with the simulation results of the proposed rate-based model. The GC can estimate the mole fraction of the solutes (acetone and acetic acid) up to the third decimal place. Each experimental run was carried out thrice, with the same feed and operating conditions. These three separate runs are reproducible within $\pm 1.5\%$ of the mole fraction of the solutes (acetine and acetic acid). The proposed mass-transfer model is based on the nonideality/nonequilibrium with respect to the proposed mass transfer and mass-transfer rate equations. The simulated mass-transfer rate profiles of the acetone (TAW system) and acetic acid (MAW systems) are shown in Figure 5 for all four runs.

Heat Transfer Features. Most of the industrial extraction columns in the petroleum industries operate in nonisothermal mode, that is, the feed and solvent enter the column at different temperatures. It also can be mentioned that both phases maintain their own distinct temperature on the stage even though they come in close contact with each other. In the thermal nonequilibrium model, the three temperatures on each of the stages are T^c, T^d, and T^I. The interface temperature T^I is not measurable, and the other two temperatures, T^c and T^d, have been measured at each stage with the help of temperature probes. Experimental temperature measurements vary within ± 0.5°C for the three repeat runs. The measured temperature profiles for Run 1 have been compared with the simulated temperature profiles in Figure 6. Simulated and experimental temperature profiles match closely. It is to be noted that a

temperature driving force of 12° to 14°C is maintained throughout the column between the two countercurrent streams. On the basis of the overall energy balance for the bench-scale experiments, the heat loss to the ambient has been estimated as 0.01% of the heat input (along with continuous and dispersed streams) at each stage; that is

$$Q^c_{Lk} = 0.01(U^+_{k-1}H^c_{k-1} + U^-_{k+1}H^c_{k+1}) \quad \text{and}$$
$$Q^d_{Lk} = 0.01(V^+_{k-1}H^d_{k-1} + V^-_{k+1}H^d_{k+1}) \quad (37)$$

Hydrodynamic Features. Comparison of concentration and the temperature profiles is not sufficient for validation of the proposed model. With the help of a digital camera, the number of drops formed on each stage has been measured for all the runs. Our computer-coded rate-based simulator can predict the drop number; the experimental and simulated drop number profiles for the two TAW runs are shown in Figure 7. The average deviation for the number of drops is ±2%. As the toluene–acetone feed mixture for the TAW system is light-dispersed, it is fed from the bottom of the column; the toluene–acetone mixture forms a coalesced layer just below the sieve trays. Similarly, the MIBK–acetic acid mixture also forms a coalesced layer below the sieve tray for the MAW system. With the help of photographic techniques and measurements, the height of this static holdup has been obtained and compared with the simulated results and is shown in Figure 8 for MAW systems. The average deviation in static holdup is ±0.5%.

In the expression for the relative velocity as proposed by Laddha and Degaleesan (1972) (Eq. B2 in Appendix B) the value of the coefficient c_{ur} was equal to 1.0. After doing sensitivity analysis in the simulation to match the experimental drop diameters and static holdups on the stages, the optimum value of c_{ur} has been obtained as 2.72. Similarly, for the dispersed phase after analyzing the experimental flow rates, the optimum diffusion coefficient is taken as 10% of the continuous phase and thus $D^d_k = 0.1 * D^c_k$.

Thermodynamic Features. The continuous and dispersed phases remain in thermal nonequilibrium, but the interface between the two phases was assumed at equilibrium. The interface at equilibrium has been modeled using thermodynamic models—UNIFAC, UNIQUAC, NRTL, and so forth. In the present work, UNIQUAC and NRTL LLE data were borrowed from DECHEMA [Macedo and Rasmussen (1987)] at the average column temperature of 40°C (UNIFAC being an approximate LLE method was not considered here for comparison). For Runs 3 and 4, the acetic acid mole-fraction profiles (both in the water phase and MIBK phase) have been compared with simulated profiles for both of the thermodynamic options. The results are shown in Figure 9. It is observed that the experimental results (acetic acid mole fraction profiles) match closely with the UNIQUAC-based simulation.

Comparison with Other Simulators. Four lab-scale experimental and simulated (with LLXSIM) results were shown earlier. To show the comparison with the other simulators, another eight TAW experiments (solvent to feed ratio and acetone compositions are given in Table 6) were considered. The mean sum of the error squares between the experimental and prediction from the simulators [LLXSIM-Debjit and Khanna (2000), CHEMSEP (1988), and ASPENPLUS (1998)] was calculated as follows

$$\text{Mean } RESQ = \left[\sum_{k=1}^{NS}\left[\frac{(z_i - z_i^{\text{expt}})}{z_i}\right]^2_k /NS\right] \quad (38)$$

where mean *RESQ* = the mean relative error square of the predicted (simulated) and the experimental mole fractions in the continuous phase. Mean *RESQ* values for the simulated runs for both the water and toluene phase are shown in Table 6. The simulated results were carried out with CHEMSEP and ASPENPLUS simulators in the equilibrium mode; LLXSIM and CHEMSEP [using the Handlos and Baron (1957) mass-transfer coefficients] in nonequilibrium mode and with both the thermodynamic options, that is, UNIQUAC and NRTL. Experimental and simulated (with different simulators—LLXSIM, CHEMSEP, and ASPENPLUS) profiles of acetone and acetic acid in the water and MIBK phases are shown in Figures 10 and 11, respectively. The MAW system is not available in CHEMSEP, so for the MAW system comparison is shown with LLXSIM and ASPENPLUS only. For the TAW system the mean value of the RESQ is even less than 0.002 for LLXSIM in both the water and toluene phase. On comparison with LLXSIM (as shown in Table 6), the mean RESQ for CHEMSEP nonequilibrium option is 100 times (of LLXSIM); for CHEMSEP and ASPENPLUS the equilibrium with UNI-

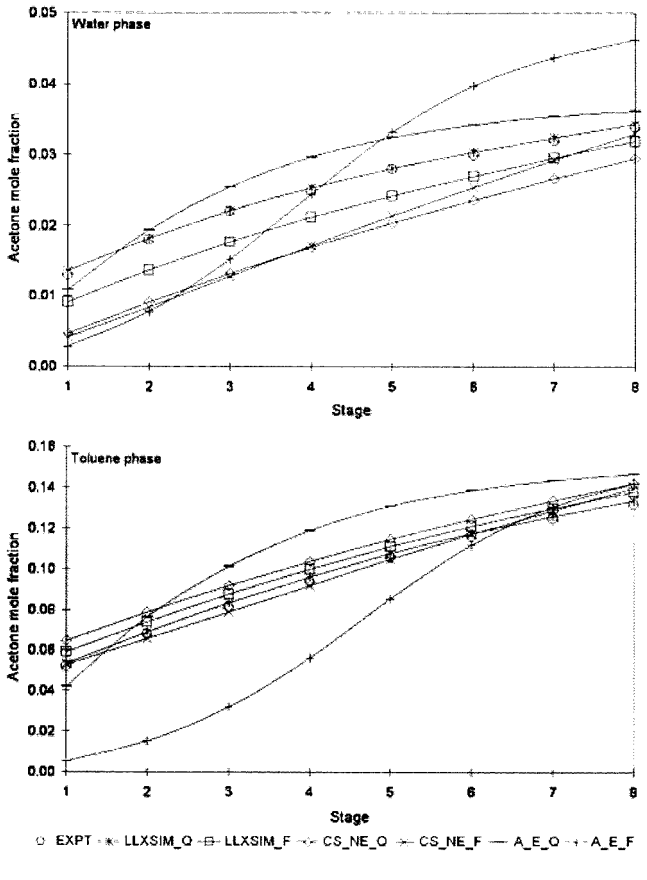

Figure 10. Acetone profiles comparison in different simulators.

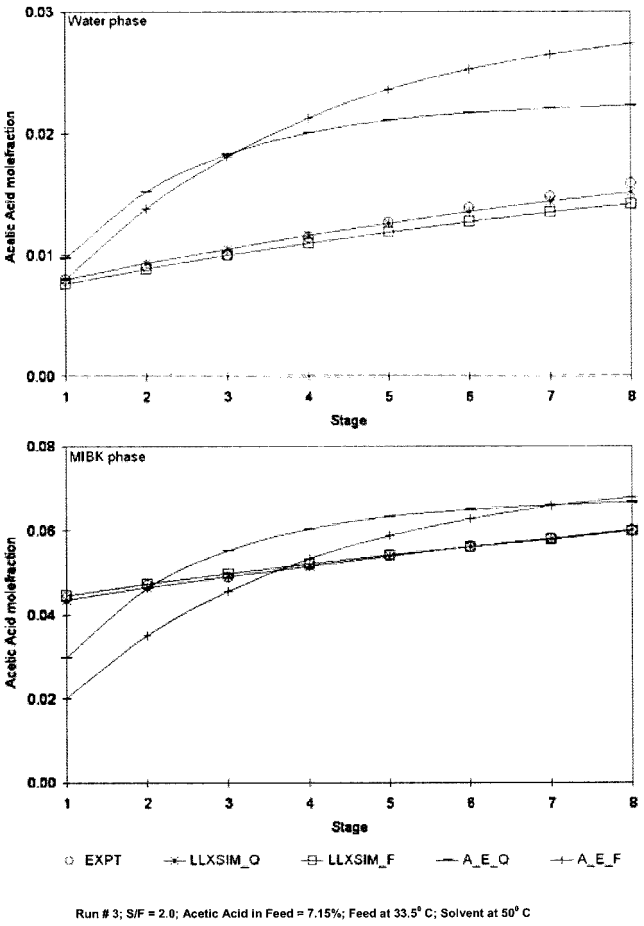

Figure 11. Acetic acid profiles comparison in different simulators.

QUAC is 50 times; and for the CHEMSEP and ASPENPLUS the equilibrium option with NRTL is 250 times.

Conclusion

An all-encompassing nonisothermal-rate-based nonequilibrium (with respect to both the mass and heat transfer) model for liquid–liquid extraction as formulated. Hydrodynamic (drop diameter, velocities, holdups, and pressure drop) and thermodynamic features (equilibrium at interface with the UNIQUAC and NRTL LLE models) for the staged extraction column were considered. To overcome the time-consuming mass-transfer and diffusion-coefficient calculations, a local mass-transfer model was proposed, resulting in time savings of a factor of 10 to 25. Validation of the developed model was achieved by conducting bench-scale nonisothermal experiments using the TAW and MAW systems. Mole fractions and temperatures in both the continuous and dispersed phases, along with a number of drops and static holdup profiles for the experimental and rate-based simulations, match closely. UNIQUAC and NRTL thermodynamic models for interface at equilibrium were compared. The mean relative error square (RESQ) for LLXSIM, the rate-based model, is about 20 to 250 times less for the various options considered than for the CHEMSEP and ASPENPLUS simulators. We are continuing the work with reactive extraction simulations and experiments in our laboratory.

Notation

a = interfacial area [m^2]
A = cross-sectional area [m^2]
A_p = preexponential frequency factor [1/s]
c = molar density or concentration [$kmol/m^3$]
C_p = molar specific heat of a pure component at any temperature T [J/mol K]
d = diameter [m]
$\mathbf{D}$ = residual vector
D = axial dispersion coefficient [m^2/s]
$Đ$ = binary diffusion coefficient in concentrated mixture [m^2/s]
$Đ^0$ = binary diffusion coefficient in infinite diluted mixture [m^2/s]
E_p = activation energy [J/kmol]
F = flow rate of feed streams [kmol/s]
$\mathbf{F}$ = vector of discrepancy functions or function residuals
G = Gibbs' free energy [J/kmol]
h = heat-transfer coefficient [J/m^2K]
$\hbar$ = height [m]
H = molar enthalpy [J/kmol]
ΔH_r = heat of chemical reaction [J/kmol]
$\mathbf{I}$ = identity matrix
$\mathbf{J}$ = Jacobian matrix
k = binary mass-transfer coefficient for [$kmol/m^2$ s]
k_p = reaction rate constant for pth term [1/s], where $p = 1$ indicates the forward reaction and $p = 2$ indicates reverse reaction; k_1 is positive and k_2 is negative
K = distribution coefficient, equilibrium ratio
l = length [m]
$\mathbf{M}$ = generalized mass-transfer coefficient matrix
n_o = number of perforations per plate
N = interphase mass-transfer rate [kmol/s]
Nu = Nusselt number
NRX = number of reversible and irreversible chemical reactions
NRC = number of components in the power-law expression
P = pressure [N/m^2]
r = chemical reaction rate [$kmol/(s \cdot m^3)$]
$\mathbf{R}$ = mass-transfer coefficient matrix
$\Re$ = resistance in mass transfer [s/kmol]
S = solvent flow rate [mol/s], entropy [J/(kmol K)]
Sh = Sherwood number
t = time [s]
T = temperature [K]
u = velocity [m/s]
U^+ = interstage backward molar flow rate of light phase [kmol/s]
U^- = interstage forward molar flow rate of light phase [kmol/s]
$\mathbf{V}$ = volume [m^3]
V^+ = interstage forward molar flow rate of heavy phase [kmol/s]
V^- = interstage backward molar flow rate of heavy phase [kmol/s]
x = mole fraction of heavy phase
$\bar{x}$ = normalized mole fraction between pair i and j
$\mathbf{X}$ = vector of unknown variables
y = mole fraction of light phase
z = generalized mole fraction

Greek letters

ε = interphase energy transfer rate [J/m^2 K]
γ = interfacial tension [N/m], activity coefficient
π = 3.14
λ = thermal conductivity [J/m K], Golden-section multiplier
$\boldsymbol{\kappa}$ = mass-transfer coefficient matrix
ρ = density of liquid [kg/m^3]
$\Delta\rho$ = positive difference in density [kg/m^3]
μ = viscosity of liquid [$kg/m \cdot s$]
ϕ = dynamic holdup volume of heavy phase [m^3 L m^3]
$\boldsymbol{\Psi}$ = matrix for the correction factor due to mass-transfer rate
φ = molar volume at phase temperature [$m^3/kmol$]
τ = tolerance
ν = stoichiometric coefficient of components in reaction, + for product, − for reactant

Superscripts and subscripts

b = bulk phase
c = continuous phase
d = dispersed phase
$expt$ = experimental
E = excess
I = interface
k = stage
m = exponent on the concentration
n = iteration number
p = phase
r = relative
c = coalescence
D = down comer
f = formation
i = component
j = component
J = jet
k = stage
l = number of reactions
m = mixture
n = variable number
N = nozzle
NC = total number of components
ND = total number of drop classes
NE = total number of equations per stage
NS = total number of stages
o = column
p = drop
ph = phenomena—formation, rise, and coalescence
r = rise
s = slip, static holdup
t = total
w = weir

Literature Cited

AspenPlus Version 10.0, developed by Aspen Technology, Inc. Cambridge, MA (1998).

ChemSep Version 3.71, CACHE Student Ed., developed by H. Kooijman, A. Haket, and R. Taylor (1988).

Chimowitz, E. H., T. F. Anderson, S. Macchietto, and L. F. Stutzman, "Local Model for Representing Phase Equilibria in Multicomponent, Nonideal Vapor Liquid and Liquid-Liquid Systems—I and II," *Ing. Eng. Chem. Process Des.,* **22,** 217 (1983) and **23,** 609 (1984).

Debjit, S., and A. Khanna, "Rate-Based and Non-Isothermal Aromatic Extraction Column Model," *Proc. PETCON,* IIT Kharagpur, India, p. 149 (2000).

Handlos, A. E., and T. Baron, "Mass and Heat Transfer from Drops in Liquid-Liquid Extraction," *AIChE J.,* **3,** 127 (1957).

Hillestad, M., C. Sorlie, T. F. Anderson, I. Olsen, and T. Hertzberg, "On Estimating the Error of Local Model Thermodynamic Models—A General Approach," *Comput. Chem. Eng.,* **13,** 789 (1989).

Incoprea, F. P., and D. P. Dewitt, *Fundamentals of Heat and Mass Transfer,* Wiley, New York (1990).

Jaiswal, A., "Simulation of a Non-Isothermal Pilot-Scale Aromatic Extraction Column," M. Tech. Thesis, IIT Kanpur, India (1999).

Kehat, E., and B. Ghitis, "Simulation of an Extraction Column," *Comput. Chem. Eng.,* **5,** 171 (1981).

Krishna, R., and G. L. Standart, "Determination of Interfacial Mass and Energy Transfer Rates for Multicomponent Vapour-Liquid Systems," *Int. Commun. Heat Mass Transfer,* **3,** 173 (1976).

Krishnamurty, R., and R. Taylor, "A Nonequilibrium Stage Model of Multicomponent Separation Process-I and II," *AIChE J.,* **31**(3), 449, 456 (1985).

Laddha, G. S., and T. E. Degaleesan, "Transport Phenomena in Liquid-Liquid Extraction," Tata McGraw-Hill, New Delhi (1976).

Lao, M., R. Krishnamurty, R. Taylor, and J. P. Kingsley, "A Non-Equilibrium Stage Model of Multi-Component Separation Process. VI—Simulation of Liquid-Liquid Extraction," *Chem. Eng. Commun.,* **86,** 73 (1989).

Macedo, E. A., and P. Rasmussen, "Liquid-Liquid Equilibrium Data Collection," *DECHEMA, Chem. Data Ser.,* **5** (Suppl. 1; Pt 4), 495 (1987).

Markowitz, H. M., "The Elimination Form of the Inverse and Its Application to Linear Programming," *Manage. Sci.,* **3,** 255 (1957).

Powers, M. F., D. J. Vickery, A. Arehole, and R. Taylor, "A Non-Equilibrium Stage Model of Multicomponent Separation Processes—V. Computational Method for Solving the Model Equations," *Comput. Chem. Eng.,* **12,** 1229 (1988).

Ricker, N. L., and C. J. King, "An Efficient General Method for Computation of Counter Current Separation Processes with Axial Dispersion," *AIChE J.,* **27,** 277 (1981).

Samant, K. D., and K. M. Ng, "Design of Multistage Extractive Processes," *AIChE J.,* **44,** 2689 (1998).

Sanpui, D., and A. Khanna, "Selection of Mass Transfer Correlations for Rate Based LLX Model," *Proc. Asia Pacific Congress for Chemical Engineering,* Christchurch, New Zealand (2002).

Siddiqi, M. A., and K. Lucas, "Correlation for Prediction of Diffusion in Liquids," *Can. J. Chem. Eng.,* **64,** 839 (1986).

Skelland, A. H. P., and W. L. Conger, "Rate Approach to Design of Perforated-Plate Extraction Columns," *Ind. Eng. Chem. Proc. Des. Dev.,* **12,** 448 (1973).

Spencer, J. L., L. Steiner, and S. Hartland, "Model Based Analysis of Data from Counter-Current Liquid-Liquid Extraction Data," *AIChE J.,* **27,** 1008 (1981).

Stadtherr, M. A., and E. S. Wood, "Sparse Matrix Methods for Equation Based Chemical Process Flowsheeting. I: Reordering Phase," *Comput. Chem. Eng.,* **8,** 9 (1984a).

Stadtherr, M. A., and E. S. Wood, "Sparse Matrix Methods for Equation Based Chemical Process Flowsheeting. II: Numerical Phase," *Comput. Chem. Eng.,* **8,** 19 (1984b).

Taylor, R., and R. Krishna, *Multicomponent Mass Transfer,* Wiley, New York (1993).

Wesselingh, J. A., and R. Krishana, *Mass Transfer,* Ellishorwood, Chichester, England (1990).

Zimmermann, A., G. Gourdon, X. Joulia, A. Gorak, and G. Cassamatta, "Simulation of Multicomponent Extraction Process by a Non Equilibrium Stage Model Incorporating a Drop Population Model," *Comput. Chem. Eng.,*Vol. 16 (Suppl.), S, 403 (1992).

Zimmermann, A., X. Joulia, G. Gourdon, and A. Gorak, "Maxwell-Stefan Approach in Extraction Design," *Chem. Eng. J.,* **57,** 229 (1995).

Zuiderweg, F. J., "Sieve Trays: A View on the State of the Art," *Chem. Eng. Sci.,* **37,** 1441 (1982).

Appendix

A. Mass-transfer correlations

It has been observed that Skelland and Conger (1973) (for k_{ij} of stagnant drops), Wesselingh and Krishna (1990) (for $Đ_{ij}$), and Siddiqi and Lucas (1986) (for $Đ^0_{ij}$) as suggested by Sanpui and Khanna (2002) are the best combination for the TAW and MAW systems.

Binary Mass-Transfer Coefficients. Skelland and Conger (1973)

drop formation

$$d\text{-}phase\colon k^d_{ijk} = 0.0423\left(\frac{d_{pk}\rho^d_k}{t_{fk}M^d_{avk}}\right) \times \left(\frac{u^2_{Nk}}{d_{pk}g}\right)^{0.089}\left(\frac{d^2_{pk}}{t_{fk}Đ^d_{ijk}}\right)^{-0.334}\left(\frac{\mu^d_k}{\sqrt{(\rho^d_k d_{pk}\gamma_k)}}\right)^{-0.6} \quad \text{(A1)}$$

$$c\text{-}phase\colon k^c_{ijk} = 0.386\left(\frac{\rho^c_k}{M^c_{avk}}\right)\left(\frac{Đ^c_{ijk}}{t_{fk}}\right)^{0.5}\left(\frac{\rho^c_k\gamma_k}{\Delta\rho_k g t_{fk}\mu^c_k}\right)^{0.407}\left(\frac{gt_{fk}}{d_{pk}}\right)^{0.148} \quad \text{(A2)}$$

drop coalescence

$$d\text{-}phase\text{: } k^d_{ijk} = 0.173\left(\frac{d_{pk}\rho^d_k}{t_{ck}M^d_{avk}}\right) \times \left(\frac{\mu^d_k}{\rho^d_k \mathcal{D}^d_{ijk}}\right)^{-1.115}\left(\frac{\Delta\rho_k g d^2_{pk}}{\gamma_k}\right)^{1.302}\left(\frac{u^2_{sk}t_{ck}}{\mathcal{D}^d_{ijk}}\right)^{0.146} \quad \text{(A3)}$$

$$c\text{-}phase\text{: } k^c_{ijk} = 0.5959\left(\frac{\rho^c_k}{M^c_{avk}}\right) \times (\mathcal{D}^c_{ijk}/t_{ck})^{0.5}\left(\frac{\rho^c_k u^3_{sk}}{g\mu^c_k}\right)^{0.332}\left(\frac{d^2_{pk}\rho^c_k\rho_c u^3_{sk}}{\mu^c_k\gamma_k}\right)^{0.525} \quad \text{(A4)}$$

circulating drop fall/rise

$$d\text{-}phase\text{: } k^d_{ijk} = 31.4\left(\frac{\mathcal{D}^d_{ijk}\rho^d_k}{d_{pk}M^d_{avk}}\right) \times \left(\frac{4\mathcal{D}^d_{ijk}t_{rk}}{d^2_{pk}}\right)^{-0.34}\left(\frac{\mu^d_k}{\rho^d_k\mathcal{D}^d_{ijk}}\right)^{-0.125}\left(\frac{d_{pk}u^2_{sk}\rho^d_k}{\gamma_k}\right)^{0.37} \quad \text{(A5)}$$

$$c\text{-}phase\text{: } k^c_{ijk} = 0.725\left(\frac{\rho^c_k}{M^c_{avk}}\right)\left(\frac{d_{pk}u_{sk}\rho^c_k}{\mu^c_k}\right)^{-0.43} \times \left(\frac{\mu^c_k}{\rho^c_k\mathcal{D}^c_{ijk}}\right)^{-0.58} u_{sk}(1-\phi_k) \quad \text{(A6)}$$

Binary Diffusion Coefficients for Concentrated Mixtures (modified expressions for multicomponent systems). Wesselingh and Krishna (1990):

$$\mathcal{D}_{ijk} = (\mathcal{D}^0_{ijk})^{(1+\bar{x}_{jk}-\bar{x}_{ik})/2}(\mathcal{D}^0_{jik})^{(1+\bar{x}_{ik}-\bar{x}_{jk})/2} \quad \text{(A7)}$$

where

$$\bar{x}_{ik} = \frac{x_{ik}}{x_{ik}+x_{jk}}, \qquad \bar{x}_{jk} = \frac{x_{jk}}{x_{ik}+x_{jk}} \quad \text{(A8)}$$

Infinite Dilution Binary Diffusion Coefficients. Siddiqi and Lucas (1986):

$$\mathcal{D}^0_{ijk} = 9.89 * 10^{-8}\mu^{-0.907}_{jk}V^{-0.45}_{ik}V^{-0.265}_{jk}T^n_k \quad \text{(A9)}$$

B. Hydrodynamic correlations

Laddha and Degaleesan (1972):
Dispersed phase velocity:

$$u^d_k = u^r_k - u^c_k \quad \text{(B1)}$$

Relative velocity:

$$u^r_k = c_{ur}(1-\phi_k)u^{r^*}_k \quad \text{(B2)}$$

Characteristic velocity:

$$u^{r^*}_k = 1.088(\gamma\Delta\rho/\rho^2_c)^{0.25}(u^2_{Nk}/2gd_{Nk})^{-0.0818} \quad \text{(B3)}$$

Nozzle velocity:

$$u_{Nk} = 2.69\left(\frac{d_{Jk}}{d_{Nk}}\right)^2\sqrt{\frac{\gamma_k/d_{pk}}{0.5137\rho^d_k + 0.4863\rho^d_k}} \quad \text{(B4)}$$

Average drop diameter:

$$d_{pk} = 1.592(\gamma_k/\Delta\rho_k g)(u^2_{Nk}/2gd_{Nk})^{-0.0665} \quad \text{(B5)}$$

Skelland and Conger (1973) proposed the expressions for slip velocity, formation, and rise time as given below:
Slip velocity:

$$u_{sk} = \left(\frac{4.0\Delta\rho_k g d_{pk}}{3.0\rho^c_k f_D}\right)^{0.5}(1-\phi_k) \quad \text{(B6)}$$

Formation time:

$$t_{fk} = \frac{(\pi/6)d^3_{pk}}{(\pi/4)d^2_N u_N} = t_{cf} \quad \text{(B7)}$$

Rise time:

$$t_{rk} = (\hbar_{tk} - \hbar_{ck})/u_{sk} \quad \text{(B8)}$$

The axial diffusion coefficient for the back mixing has been used analogous to the vapor–liquid system suggested by Zuiderweg (1982) as shown below:
c-phase:

$$D^c_k = 8.3\left(\frac{u^{c2}_k\rho^c_k}{u^d_k\rho^d_k}\right)(l_w/A_p)\hbar^2_k \quad \text{(B9)}$$

Pressure Drop on Stage.
Static pressure drop:

$$\Delta P_s = h_s\rho^d_k g \quad \text{(B10)}$$

Dynamic volume for stage:

$$\mathbf{V}_{dyn\,k} = \mathbf{V}_k - A_0\hbar_s \quad \text{(B11)}$$

Dynamic height for stage:

$$\hbar_{dyn\,k} = n_0\frac{\pi}{6}d^3_{pk}/\mathbf{V}_{dyn\,k} \quad \text{(B12)}$$

Mixture density for stage:

$$\rho^m_k = \hbar_{dyn}\rho^d_k + (1-\hbar_{dyn})\rho^c_k \quad \text{(B13)}$$

Pressure drop due to dynamic holdup:

$$\Delta P_{dyn,k} = (\hbar_k - \hbar_s)\rho_k^m g \tag{B14}$$

Total pressure drop on stage:

$$\Delta P_k = \Delta P_s + \Delta P_{dyn,k} \tag{B15}$$

Pressure on stage:

$$P_k = P_{k-1} + \Delta P_k \tag{B16}$$

C. Heat-transfer correlations

Enthalpy with Heat of Mixing.
Enthalpy for the stream:

$$H_k^p = \sum_{i=1}^{NC} x_{ik} H_i^0 + \Delta H_{mk}^p \tag{C1}$$

Heat of mixing:

$$\Delta H_{mk}^p = \Delta G_{mk}^p + T_k^p \Delta S_{mk}^p \tag{C2}$$

where mixture Gibbs' energy

$$\Delta G_{mk}^p = G^E + \Delta G_{mk}^{Ideal} = RT_k^p \left(\sum_{i=1}^{NC} z_{ik}^p \ln \gamma_{ik}^p - \sum_{i=1}^{NC} z_{ik}^p \ln z_{ik}^p \right)$$

and mixture entropy

$$\Delta S_{mk}^p = S^E + \Delta S_{mk}^{Ideal} = R \left(\sum_{i=1}^{NC} z_{ik}^p \ln \frac{\varphi_{ik} z_{ik}^p}{\sum_{j=1}^{NC} \varphi_{jk} z_{jk}^p} - \sum_{i=1}^{NC} z_{ik}^p \ln z_{ik}^p \right)$$

Heat-Transfer Coefficients.
Incropera and Dewitt (1990):

$$h_k^c = Nu_k^c (\rho_k^c u_k^c C_{pk}) \qquad \text{for } c\text{-phase} \tag{C3}$$

Taylor and Krishna (1993):

$$h_k^d = (2/3)\pi^2 \lambda_k^d / d_{pk} \qquad \text{for } d\text{-phase} \tag{C4}$$

where

$$Nu_k^c = [2.06 (d_{pk} u_k^c \rho_k^c / \mu_k^c)^{-0.575} / (1.0 - \phi_k)] / (C_{pk}^c \mu_k^c / \lambda_k^c)^{2/3}$$

Mass-Transfer Coefficient Matrix. The mass-transfer coefficient matrices can be written as follows:

$$[\boldsymbol{\kappa}]_k^p \cdot a_k = [[\mathbf{R}]_k^p]^{-1} \cdot a_k [\boldsymbol{\Psi}]_k^p \{\exp[\boldsymbol{\Psi}]_k^p - [\mathbf{I}]_k\}^{-1} [\boldsymbol{\Gamma}]_k^p \tag{C5}$$

where the elements of $[\mathbf{R}]_k^p$ and $[\boldsymbol{\Psi}]_k^p$, in terms of general mole fractions z_i and mass-transfer rate N_{ik} as suggested by Krishna and Standart (1976), are

$$\frac{[\mathbf{R}]_k^p}{a_k} = [\mathbf{M}]_k^p \tag{C6}$$

where $m_{ik} = z_{ik}$.

$$[\boldsymbol{\Psi}]_k^p = [\mathbf{M}]_k^p \tag{C7}$$

where $m_{ik} = N_{ik}$. The terms of the generalized matrix will be:

$$(M_{ii})_k^p = \frac{m_{ik}}{(k_{iNC\,ph})_k^p a_k} + \sum_{\substack{j=1 \\ j \neq i}}^{NC} \frac{m_{jk}}{(k_{ij\,ph})_k^p a_k} \tag{C8}$$

where $i = 1, 2, \ldots, (NC - 1)$.

$$(M_{ij})_k^p = -m_{ik} \left[\frac{1}{(k_{ij\,ph})_k^p a_k} - \frac{1}{(k_{iNC\,ph})_k^p a_k} \right] \tag{C9}$$

where $i \neq j$ and $i = 1, 2, \ldots, (NC - 1)$.

Manuscript received Jan. 14, 2003, and revision received June 21, 2003.